ERROR ANALYSIS IN THE JOINT EVENT LOCATION/SEISMIC CALIBRATION INVERSE PROBLEM

William Rodi

Massachusetts Institute of Technology

Sponsored by Air Force Research Laboratory

Contract No. F19628-03-C-0109

ABSTRACT

This project is developing new mathematical and computational techniques for analyzing the uncertainty in seismic event locations, as induced by observational errors and errors in travel-time models. The analysis is being done in the context of the multiple-event inverse problem, in which the locations of multiple events are inferred jointly with travel-time corrections for the event-station paths. The premise is that one of the events is the target of the uncertainty analysis while the others are calibration events that serve to constrain the path corrections within some level of error. An uncertainty analysis on the coupled location/calibration inverse problem leads to the notion of a "multiple-event" confidence region on the target event location, which accounts implicitly for errors in the inferred path corrections, including the effects of uncertainty in the calibration event locations. The approach we have developed considers the nonlinearity of the forward problem and allows the use of non-Gaussian models for data errors and soft or hard constraints on the problem parameters.

The project has addressed mainly the basic multiple-event location problem, wherein travel-time corrections comprise a simple time term for each station/phase combination in the data set. We have developed a numerical scheme for computing multiple-event confidence regions for this problem, based on grid search and Monte Carlo sampling techniques. Given the computationally intensive nature of the approach, some approximations were developed to reduce the computational effort. Experiments with data from the Nevada Test Site validated the approach and demonstrated the adequacy of the approximations when the location uncertainty is not too large. A modification of the approach we are investigating, which offers the possibility of additional efficiency, is the computation of multiple-event confidence regions defined in a Bayesian sense. Moreover, we are investigating an extension of our multiple-event location algorithm to the case where travel-time corrections are parametrized as a function of the event location.

OBJECTIVE

This project is developing new mathematical and computational techniques for quantifying the errors in seismic event locations, including the effects of observational errors and errors in the travel-time forward model. Our approach associates the latter, or *model errors*, with the uncertainty in path travel-time corrections that have been inferred from calibration data. We thus analyze event location uncertainty in the context of the joint location/calibration inverse problem: using arrival time data from multiple events and stations to simultaneously locate the events and estimate calibration parameters that determine the travel-time corrections. Calibration parameters can be as simple as time terms at stations or as complex as a 3D velocity model. Our approach treats one of the multiple events as a new event under investigation and the remaining events as calibration events. Performing uncertainty analysis on the joint location/calibration problem accounts for the key sources of error in the new event location, including picking errors in the arrival times for the new *and* calibration events and errors in the calibration event locations. We are addressing this joint inverse problem with numerical techniques, like grid search and Monte-Carlo simulation, that avoid the limitations of analytic approaches to uncertainty analysis in large inverse problems. These limitations include the restriction to Gaussian data errors, the necessity of using a linear approximation to the travel-time forward model, and restricted mechanisms for incorporating *a priori* constraints on the unknowns.

In previous years' efforts, we implemented and tested this approach to event location uncertainty for a relatively simple, but widely used, parameterization for travel-time corrections (time terms). These efforts demonstrated the conceptual validity of the approach, which could be validated quantitatively in simple situations but which revealed the practical difficulties associated with its computational intensity. Here we report on some incremental improvements to the uncertainty algorithm we have developed.

RESEARCH ACCOMPLISHED

Summary of Approach

Rodi (2004, 2005) presented the mathematical formulation of the joint location/calibration inverse problem and maximum-likelihood uncertainty approach that are the basis for this project. To summarize, we write the joint inverse problem as

$$d_{ij} = T_j(\mathbf{x}_i) + t_i + c_{ij} + e_{ij}\,, \tag{1}$$

where i indexes each of m seismic events and j indexes each of n station/phase combinations that have been observed from one or more of the events. Then, d_{ij} denotes the arrival-time observation for the ith event and jth station/phase ((i,j)th path), $\mathbf{x}_i$ and t_i are the origin parameters (hypocenter and time, respectively) of the ith event, T_j is a model-based travel-time function for the jth station/phase, c_{ij} is a correction to this function for path (i,j), and e_{ij} is an observational error. This equation holds only for the paths (i,j) for which data have been observed. The joint location/calibration problem is often referred to as the *multiple-event location* problem. The project has focused on the "basic" multiple-event location problem whereby the path corrections are assumed to be event-independent (see Jordan and Sverdrup, 1981, and Pavlis and Booker, 1983):

$$c_{ij} = a_j\,. \tag{2}$$

The unknown parameters of the inverse problem are then the event hypocenters and origin times, $\mathbf{x}_i$, t_i, $i = 1,\ldots,m$, and the time terms for the station/phase combinations: a_j, $j = 1,\ldots, n$.

The premise of our approach is that one of the events (e.g., $i = 1$) is the target of the location uncertainty analysis, while the remaining events ($i = 2,\ldots,m$) are calibration events, whose data provide information about the a_j. Generally, prior information is available to constrain the location of one or more of the calibration events.

The likelihood function for the multiple-event location problem is determined, in part, by the assumed probability distribution of the observational errors in the data, e_{ij}. We take this to be a *generalized Gaussian* distribution of order p (Billings et al, 1994). Additionally, the likelihood function depends on the prior information available for the calibration event locations. Rodi (2005) discusses the use of hard and soft prior constraints on an event location.

The latter, which we consider in this paper, take the form of a prior probability distribution on the event hypocenter. As with the data errors, we allow this distribution to be of the generalized Gaussian type.

Given these assumptions, the likelihood function for the basic multiple-event location problem is given by

$$-\log L = \text{const} + \frac{1}{p}\sum_{ij}\frac{1}{\left(\sigma_{ij}\right)^{p}}\left|d_{ij} - T_j\left(\mathbf{x}_i\right) - t_i - a_j\right|^{p} + \sum_{i}\frac{1}{p_{0i}\left(\sigma_{ij}\right)^{p_{0i}}}\left\|\mathbf{x}_i - \mathbf{x}_{0i}\right\|^{p_{0i}} , \tag{3}$$

where || || denotes the Euclidean distance in space. The prior information on the ith event location is specified by a prior location estimate, $\mathbf{x}_{0i}$; a standard error, σ_{0i}; and a generalized Gaussian order, p_{0i}, where we generally assume $p_{0j} \geq 2$. The generalized Gaussian order for the data errors is p ($1 \leq p \leq 2$), and the data standard errors are σ_{0i}. For the purpose of exposition, we assume the data standard errors are known.

Location Confidence Regions

Our approach to uncertainty analysis in the joint location/calibration inverse problem separates the unknown parameters into two vectors: **p**, containing the subset of "target" parameters on which a confidence region is desired—and **q**, containing the remaining "nuisance" parameters. For example, if $\mathbf{p} = \mathbf{x}_1$ (the hypocenter of the target event) then

$$\mathbf{q} = (t_1, \mathbf{x}_2, t_2, \ldots, \mathbf{x}_m, t_m, a_1, a_2, \ldots, a_n) . \tag{4}$$

To consider a confidence region on the *epicenter* of the target event, we would move its depth parameter, z_1, from **p** to **q**. Given this separation of parameters, we will show the likelihood function as $L(\mathbf{p},\mathbf{q};\mathbf{d})$, where **d** denotes the vector of arrival-time observations, d_{ij}.

A confidence region on **p** is determined by the behavior of the likelihood function L as a function of **p**, encompassing the points that yield the largest values of L. Throughout this project, we have defined such regions using the approach of Neyman-Pearson (N-P) hypothesis testing. We take as a test statistic, $\tau(\mathbf{p},\mathbf{d})$, the log likelihood ratio given by

$$\begin{aligned}\tau(\mathbf{p},\mathbf{d}) &= \log\max_{\mathbf{p},\mathbf{q}} L(\mathbf{p},\mathbf{q};\mathbf{d}) - \log\max_{\mathbf{q}} L(\mathbf{p},\mathbf{q};\mathbf{d}) \\ &\equiv \log L(\mathbf{p}^*,\mathbf{q}^*;\mathbf{d}) - \log\max_{\mathbf{q}} L(\mathbf{p},\mathbf{q};\mathbf{d}).\end{aligned} , \tag{5}$$

where $(\mathbf{p}^*,\mathbf{q}^*)$ denotes the maximum-likelihood solution for the parameters. We see that τ compares the likelihoods that are achieved with **p** fixed to a particular value (second term of τ) and with **p** free to vary (first term). In each case **q** is free. A N-P confidence region on **p** at confidence level β (e.g. $\beta = 95\%$) is the locus of points satisfying

$$\tau(\mathbf{p}, \mathbf{d}) \leq \tau_\beta(\mathbf{p}) , \tag{6}$$

where $\tau_\beta(\mathbf{p})$ is a critical value of the probability distribution of τ, as induced by the distribution of the data errors:

$$\text{Prob}\left\{\tau(\mathbf{p}, \mathbf{d}) \leq \tau_\beta(\mathbf{p}) \mid \mathbf{p}\right\} = \beta. \tag{7}$$

In writing this and Equation (6), we have allowed for the possibility that the distribution of τ may depend on **p**, but we have tacitly assumed that is does not depend on the nuisance parameters.

We have developed a two-step numerical algorithm to implement the N-P approach to confidence regions. The first step maps the test-statistic, $\tau(\mathbf{p}, \mathbf{d})$, on a grid in **p**-space. This entails minimizing the likelihood function with respect to **q** with **p** fixed in turn to each point on the grid. The second step performs Monte Carlo simulation to infer the critical values $\tau_\beta(\mathbf{p})$. This entails maximizing L with respect to **q**, with **p** fixed and free, for each of many realizations of synthetic data. Both steps of this algorithm are computationally intensive because they involve repeated

maximization of L, i.e., repeated solution of a multiple-event location problem involving many location and calibration parameters.

Needless to say, this formulation applies to the single-event location problem and "single-event confidence regions" by removing the travel-time corrections, a_j, and the calibration events and their data from the problem (i.e., $a_j = 0$, $m = 1$).

Monte Carlo Short Cuts

When data and prior errors are Gaussian ($p = p_{0i} = 2$) and when the model-based travel-time functions can be approximated as linear, τ_β does not depend on **p**. In general, however, τ_β might depend on **p,** indicating the need to perform a separate Monte Carlo simulation with each value of **p** on the sampling grid used for the "true" parameters in calculating synthetic data realizations. This is not practical for realistic problems, and our algorithm performs Monte Carlo simulation only with **p** set to its maximum-likelihood estimate, **p***. That is, Equation (6) is replaced with

$$\tau(\mathbf{p}, \mathbf{d}) \le \tau_\beta(\mathbf{p}^*). \tag{8}$$

This approximation has been assumed by others who have computed numerical confidence regions on seismic event locations (e.g., Wilcock and Toomey, 1991). However, to the extent that the dependence on **p** exists, the confidence regions based on Equation (8) lose the "confidence property," i.e., the region includes the true parameter vector with probability β, regardless of what the true parameter vector is.

A second significant short cut we have implemented pertains to the nuisance parameters. In the Gaussian/linear case, the probability distribution of τ (which is chi-squared) depends only on the dimensionality of **p**, regardless of what, if any, nuisance parameters there are. As a result, **q** can be ignored for the purpose of determining τ_β. In a Monte Carlo simulation of τ_β, this implies that the likelihood maximization with synthetic data realizations can treat **q** as fixed. In the location/calibration problem, most of the computational benefit of doing this is achieved by fixing the calibration event locations so that each likelihood maximization involves the work of single-event, rather than multiple-event, location.

Quasi-Bayesian Confidence Regions

In Bayesian inference, the likelihood function we defined in Equation (3), including the factor for prior information on the parameters, is treated as an unnormalized *posterior* probability density function on the parameters. A Bayesian confidence region on **p** at confidence level β is a region in **p**-space, P_β, which includes a proportion β of the posterior probability density:

$$\int_{P_\beta} d\mathbf{p} \int_{Q_1} d\mathbf{q} L(\mathbf{p}, \mathbf{q}; \mathbf{d}) = \beta \int_{P_1} d\mathbf{p} \int_{Q_1} d\mathbf{q} L(\mathbf{p}, \mathbf{q}; \mathbf{d}), \tag{9}$$

where P_1 and Q_1 denote the entire **p**-space and **q**-space, respectively. In a Gaussian/linear problem, Bayesian confidence regions coincide with N-P regions and thus posses the confidence property. In general, however, the two types of regions differ, and Bayesian ones do not necessarily have the confidence property.

The difference between N-P and Bayesian confidence regions in the presence of nonlinearity is illustrated in Figure 1. This is a "toy" problem involving one unknown parameter—event depth—and a single datum that is taken to be a direct estimate of the depth. We introduce nonlinearity into the problem in the form of the hard constraint that the true event depth (horizontal axis) cannot be negative, even though the depth estimate (vertical axis) might be, such as when arrival times yield an "airquake" as the best-fitting solution for an event location. Intuitively, the positivity constraint on depth should affect a confidence region on depth when the depth estimate is near $z = 0$, and we can see from the figure that it does. The case in the left panel assumes that the depth estimate has a Gaussian distribution ($p = 2$) while the case on the right assumes a Laplace distribution ($p = 1$). The green lines in each plot trace the confidence limits for a N-P confidence intervals, which possess the confidence property. The red dots are

the approximate N-P confidence intervals that result when the critical value τ_β is considered only for the estimated (maximum-likelihood) value of depth, as per Equation (8), and the blue dots mark the Bayesian confidence limits. Generally, the approximate N-P intervals are smaller than the Bayesian intervals for shallow depth estimates, showing they are more influenced by the positivity constraint. Which one better represents the exact N-P intervals depends on the type of data distribution used.

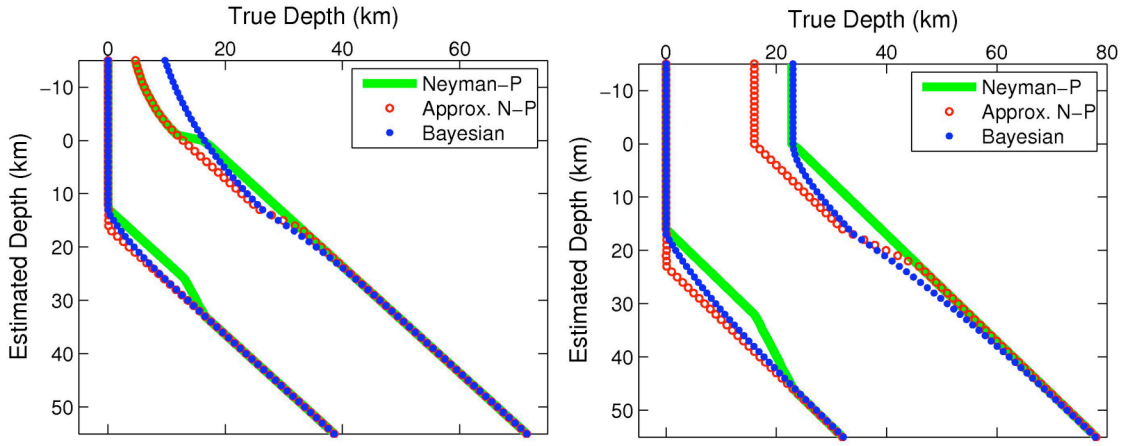

Figure 1. Confidence intervals on event depth in a fictitious problem involving a direct estimate of depth, which is either Gaussian (left panel) or Laplace (right) distributed, with a standard error of 10 km in each case. Three types of confidence limits (at β = 90%) are shown, each as a function of the depth estimate itself (vertical axis): exact N-P (green line), approximate N-P (red dots), and Bayesian (blue dots). The corresponding confidence interval is the range of true depth between these limits.

It is straightforward to modify our numerical algorithm to compute Bayesian confidence regions if we make an additional approximation, namely, replacing the integration over the nuisance parameters **q** in Equation (9) with maximization. (Acknowledging this approximation, we will call the resulting confidence regions "quasi-Bayesian.") Considering the definition of τ in Equation (5), Equation (9) becomes equivalent to Equation (6), with a single τ_β computed as the solution of

$$\int_{\tau(\mathbf{p},\mathbf{d})\le\tau_\beta} d\mathbf{p}\, e^{-\tau(\mathbf{p},\mathbf{d})} = \beta \int_{\tau(\mathbf{p},\mathbf{d})<\infty} d\mathbf{p}\, e^{-\tau(\mathbf{p},\mathbf{d})}. \qquad (10)$$

Application to NTS Data

We are testing our new uncertainty analysis techniques on regional seismic arrival times from NTS explosions, for which precise locations and origin times are known (Walter et al., 2003). The results shown here are based on a subset of the available data set, comprising 262 Pn arrivals from 33 explosions at Pahute Mesa and Rainier Mesa. This subset included arrivals from the 27 stations that spanned the epicentral distance range 1,5°–9° and had Pn arrivals for at least 2 of the 33 events.

When computing a confidence region on the location of one of the events (the "target" event), the remaining 32 events were treated as calibration events. Only one calibration event was assigned a finite ground truth (GT) level; a relatively well-recorded Rainier Mesa explosion (16 Pn arrivals). Its assigned GT accuracy was varied between 0 and 5 km. The depths of all events were fixed to their true values in these tests. The origin times of all events, including the GT calibration event, were unconstrained. The IASP91 travel-time tables were used for the forward model.

Figure 2 compares the epicenter solutions obtained with single-event location (zero travel-time corrections) with multiple-event solutions obtained with varying GT levels for the GT-calibration event. We see that the multiple-event solutions achieve greater accuracy in the *relative* locations between events, but the absolute event mislocations become larger as the location constraint on the GT-calibration event is relaxed.

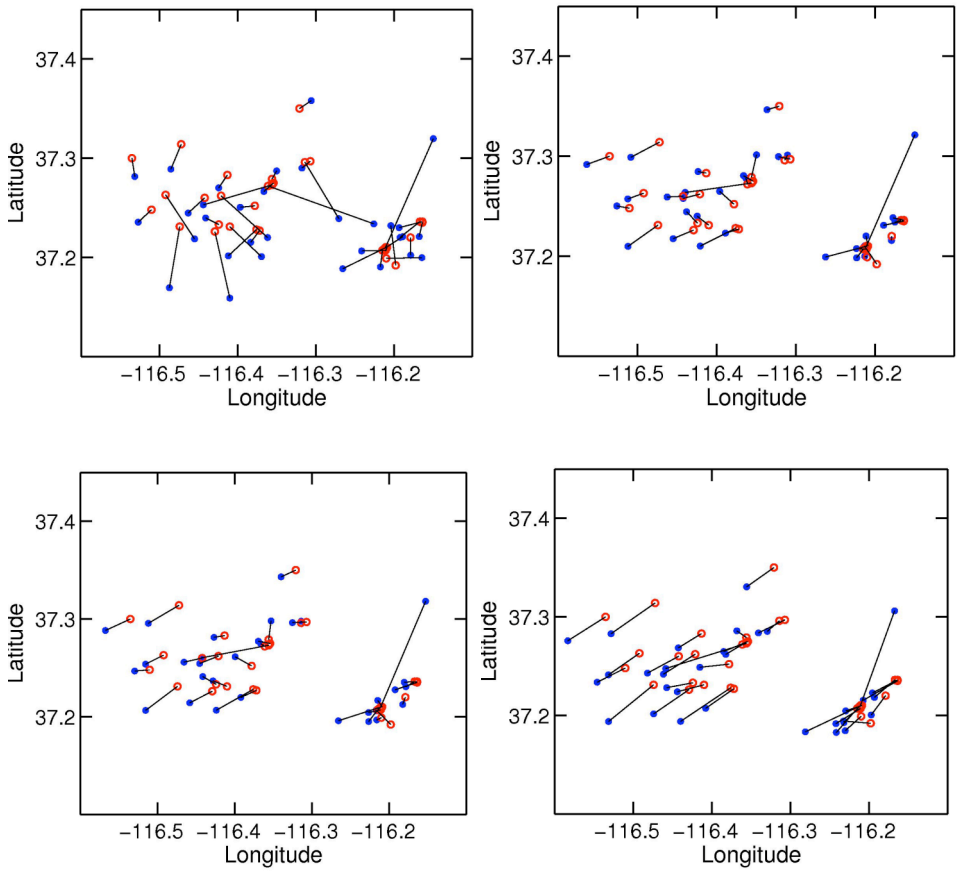

Figure 2. Four epicenter solutions for 33 NTS explosions in the Pahute Mesa and Rainier Mesa testing areas. Each solution location (blue dot) is connected by a line to the corresponding true (GT0) epicenter of the event (red circle). Top left: Solution obtained with single-event location (travel-time corrections set to zero). Top right: Solution obtained with multiple-event location with the location of one well-recorded Rainier Mesa event (37.21°N, 116.21°W) held fixed (GT0 constraint). Bottom: Multiple-event location solutions with the same Rainier Mesa event treated as GT2 (bottom left) and GT5 (bottom right).

Single-Event and Multiple-Event Confidence Regions

Figure 3 compares single-event and multiple-event confidence regions for a Pahute Mesa event with relatively few arrivals (6 Pn arrivals). The regions were calculated using a Gaussian distribution for observational errors ($p = 2$). The colored areas are the confidence regions, for different confidence levels, computed with our two-step (approximate N-P) numerical algorithm. The single-event regions (left) do not include the effect of errors in travel-time corrections (model errors) and agree almost exactly with analytically derived confidence ellipses based on only the picking error variance (shown for $\beta = 95\%$).

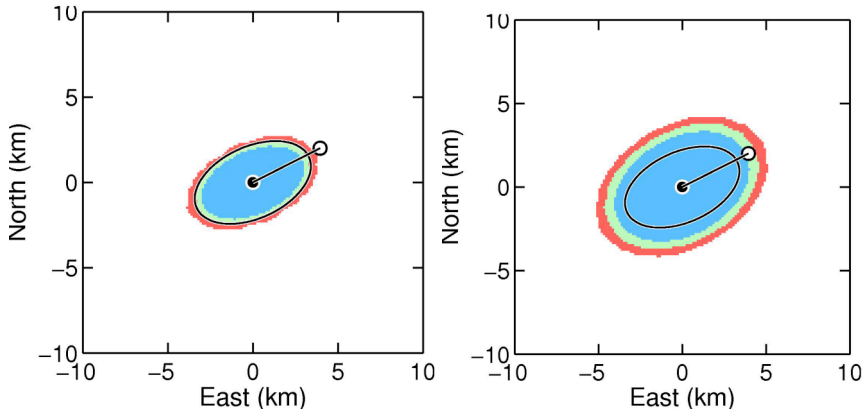

Figure 3. Epicenter confidence regions for a Pahute Mesa explosion with 6 Pn arrivals, computed with our two-step numerical algorithm. Left: Single-event confidence regions (path travel-time corrections assumed known). Right: Multiple-event confidence regions, treating a well-recorded Rainier Mesa event as a GT0 calibration event. Confidence regions are shown for 90%, 95%, and 98% confidence (blue, green, and red, respectively). In each frame the black circle marks the maximum-likelihood solution for the event location, and the white circle is its GT0 location (from Walter et al., 2003). The error distribution for picking errors was assumed to be Gaussian ($p = 2$). The ellipse in each frame is the conventional 95% *single-event* confidence ellipse, computed analytically under the Gaussian/linear assumption.

The multiple-event confidence regions (right panel) are larger because they account for the additional location uncertainty induced by uncertainty in the estimated travel-time corrections. The multiple-event confidence regions in this case assumed that the GT event at Rainier Mesa was GT0. Therefore, the confidence regions do not account for any location uncertainty in this calibration event.

Monte Carlo Simulation vs. Likelihood Integration

Figure 4 shows multiple-event confidence regions for the same Pahute Mesa target event just considered, computed two different ways. The results in the top row used the same two-step procedure used for Figure 3 (approximate N-P confidence regions). The results in the bottom row are quasi-Bayesian (q-B) confidence regions. The two types of confidence regions are generated from the same numerical mapping of the test statistic (τ) as a function of epicenter, but they use different critical values of the test statistic (τ_β) to determine which contour of τ corresponds to each confidence level. The N-P regions determine τ_β with Monte Carlo simulation (doing 500 realizations), while the q-B regions use likelihood integration, as discussed earlier.

The left panels of Figure 4 assume a GT0 calibration event (the top left panel repeats the right panel of Figure 3.) The center and right panels, respectively, assume the GT-calibration event is GT2 and GT5. We see that the confidence regions grow as the GT level is increased (see Rodi (2005) for additional examples). Comparing the two methods (top vs. bottom panels), we see that the quasi-Bayesian confidence regions are smaller. This owes to the fact that likelihood integration yielded smaller values of τ_β than did Monte Carlo simulation.

Table 1 compares the critical statistics determined by the two methods with the value predicted by the Gaussian/linear theory. The critical values from likelihood integration and the linear/Gaussian theory agree in both the single-event and multiple-event cases, but the Monte Carlo values are larger than either in the multiple-event cases. A discrepancy from the Gaussian/linear values can only be due to nonlinearity (since Gaussian data and prior errors were assumed). However, we would expect the effect of nonlinearity to increase as the GT level of the GT-calibration event increases, but the Monte-Carlo values do not increase. Based on this comparison, we tentatively prefer the likelihood-integration method for determining τ_β. The remaining examples of this paper show quasi-Bayesian confidence regions.

Table 1. Comparison of critical τ values from Monte Carlo simulation (M.C.), likelihood integration (L.I.) and Gaussian/linear theory $\left(\frac{1}{2}\chi_2^2\right)$

	$\beta = 90\%$			$\beta = 95\%$		
Case	M.C.	L.I.	$\frac{1}{2}\chi_2^2$	M.C.	L.I.	$\frac{1}{2}\chi_2^2$
S-E	2.34	2.27	2.30	2.89	2.94	3.00
M-E (GT0)	2.86	2.31	2.30	3.66	2.98	3.00
M-E (GT2)	2.87	2.37	2.30	3.66	3.09	3.00
M-E (GT5)	2.87	2.29	2.30	3.65	3.01	3.00

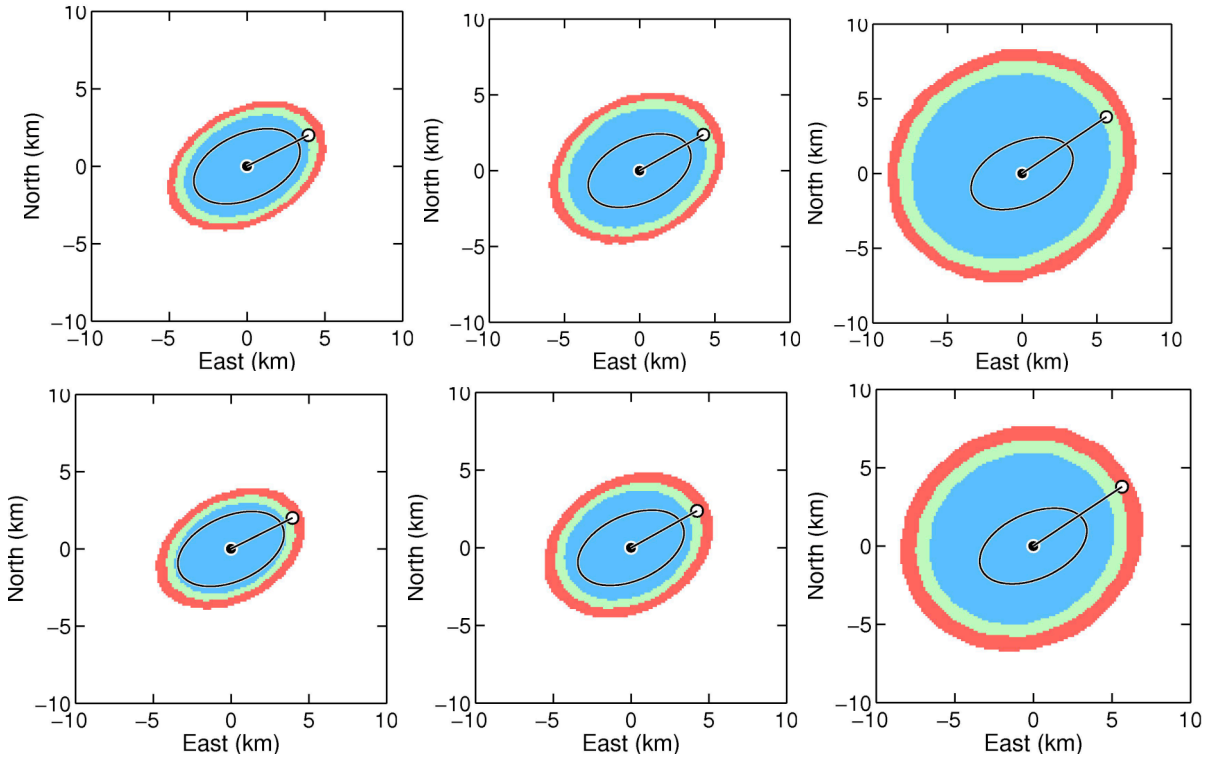

Figure 4. Approximate N-P (top) and quasi-Bayesian (bottom) multiple-event confidence regions for the same Pahute Mesa explosion considered in Figure 3. The Rainier Mesa GT-calibration event is assumed to be GT0 (left), GT2 (center), or GT5 (right). A Gaussian error model is used for both the picking errors and the prior location error ($p = p_0 = 2$). Plotting conventions are the same as Figure 3.

Non-Gaussian Error Models

The examples shown above assumed Gaussian data errors ($p = 2$) and a Gaussian prior error on the GT-calibration event at Rainier Mesa ($p_0 = 2$). Using other tests with NTS data, Rodi (2005) showed that increasing p_0 ("hardening" the GT constraint) caused confidence regions to become non-elliptical, especially in the GT5 case. Figure 5 illustrates this for the target event we have been considering.

Our final test shows the effect of using a non-Gaussian probability distribution for the observational errors. Figure 6 shows single-event and multiple-event confidence regions (same target event) for two values of the generalized Gaussian distribution: $p = 1.5$ (top) and 1.25 (bottom). The confidence regions depart from an elliptical shape more

for p = 1.25 (bottom panels) than for p = 1.5, as expected. The non-ellipticity is most noticeable in the single-event regions, which are most strongly influenced by the picking error distribution.

These results also show the numerical challenge of automatically, but efficiently, gridding the test statistic when its behavior departs significantly from a quadratic function (see lower panels). Our current scheme designs a mapping grid in advance (guided by the conventional error ellipse parameters), but these tests indicate the need for an adaptive gridding scheme.

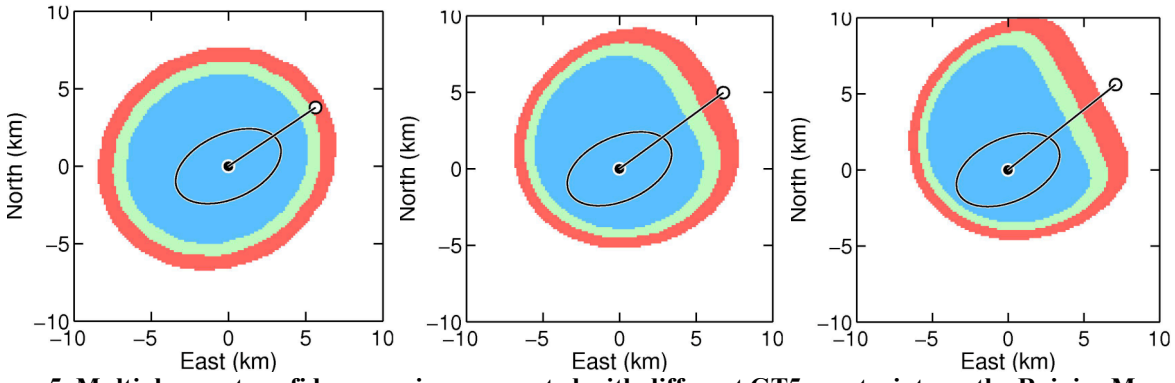

Figure 5. Multiple-event confidence regions computed with different GT5 constraints on the Rainier Mesa calibration event: generalized Gaussian orders p_0 = 2, 5, and 20 (left, center, and right, respectively). The GT5 constraint is at 90% confidence in each case. The data errors are assumed to be Gaussian. The target event is the same as in previous figures.

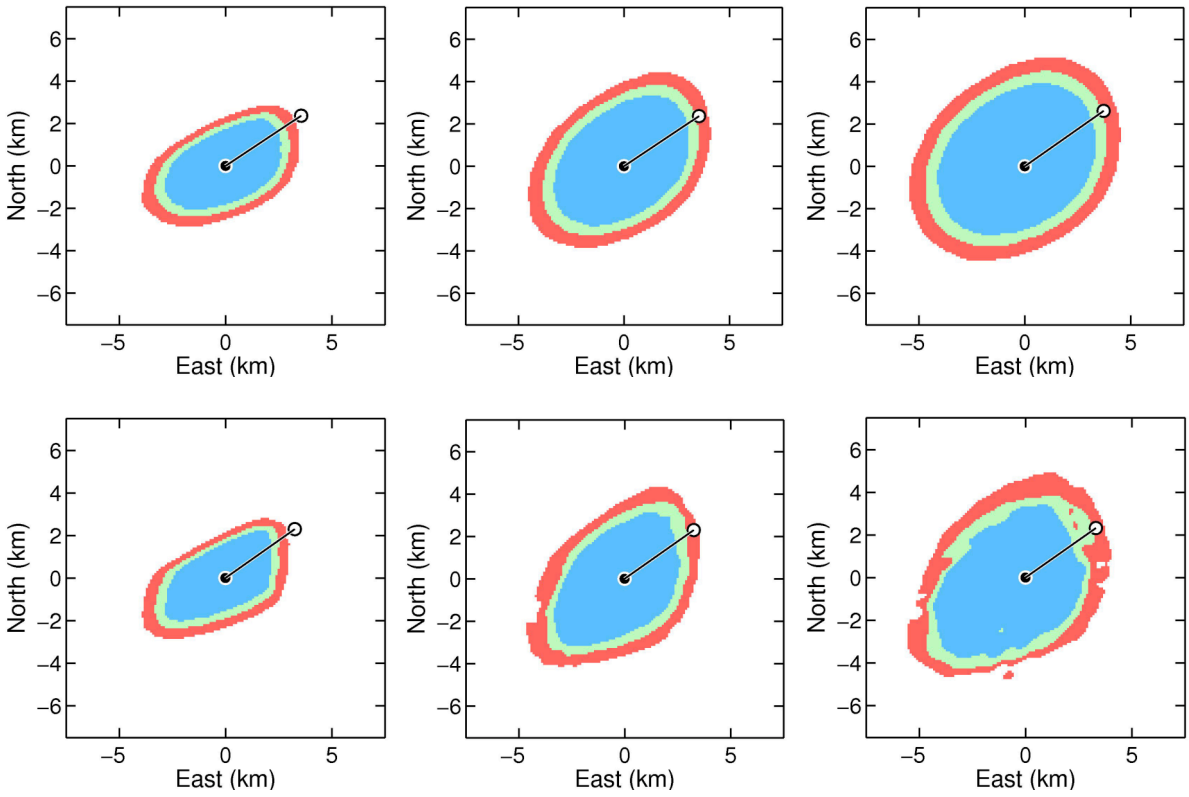

Figure 6: Single-event (left) and multiple-event confidence regions computed using two non-Gaussian probability distributions for picking errors: generalized Gaussian orders p =1.5 (top) and 1.25 (bottom). The prior error on the GT-calibration event for the multiple-event regions is either GT0 (center panels) or GT2 (right), with a Gaussian prior error assumed for the latter.

CONCLUSIONS AND RECOMMENDATIONS

The project has made significant progress in the development of a new approach to event location uncertainty analysis. The approach is based on the framework of the joint location/calibration inverse problem, which considers the effects of both picking and model errors on event location errors. We have implemented numerical techniques for computing "multiple-event" confidence regions without need of the conventional assumptions of Gaussian errors and linearity of the forward problem. Our recent work has focused on additional enhancements to the computational efficiency of the approach, which have led to the alternative of using likelihood integration to replace the Monte Carlo simulation step of our original algorithm. This alternative is tantamount to a Bayesian approach to uncertainty but can also be viewed as just a different computational short cut for approximating the exact confidence regions defined by N-P hypothesis testing. Our results to date suggest that this new approximation may in fact be more accurate. It is apparent, however, that further work is needed to produce reliable calculations when error distributions depart significantly from Gaussian and confidence regions from ellipses.

The practicality of our approach for more complex parameterizations of travel-time corrections, such as velocity models, is in question at this point. However, our future plans include pursuing a more-efficient scheme for generating likelihood functions on a grid (e.g., using linearization with respect to "nuisance" parameters), and this may alter the outlook. In any event, extending our approach to more-complex parameterizations remains a feasible task for research that we intend to pursue during the final year of the project.

REFERENCES

Billings, S. D., M. S. Sambridge, and B. L. N. Kennett (1994). Errors in hypocenter location: Picking, model and magnitude dependence, *Bull. Seism. Soc. Am.* 84: pp. 1,978–1,990.

Jordan, T. H. and K. A. Sverdrup (1981). Teleseismic location techniques and their application to earthquake clusters in the south-central Pacific, *Bull. Seism. Soc. Am.* 71: pp. 1,105–1,130.

Pavlis, G. L. and J. R. Booker (1983). Progressive multiple event location (PMEL), *Bull. Seism. Soc. Am.* 73: pp. 1753–1777.

Rodi, W. (2004). Error analysis in the joint event location/seismic calibration inverse problem, in *Proceedings of the 26th Seismic Research Review: Trends in Nuclear Explosion Monitoring*, LA-UR-04-5801, Vol. 1, pp. 307–316.

Rodi, W. (2005). Error analysis in the joint event location/seismic calibration inverse problem, in *Proceedings of the 27th Seismic Research Review: Ground-Based Nuclear Explosion Monitoring Technologies*, LA-UR-05-6407, Vol. 1, pp. 433–442.

Walter, W. R., K. D. Smith, J. L. O'Boyle, T. F. Hauk, F. Ryall, S. D. Ruppert, S. C. Myers, M. Anderson, and D. A. Dodge (2003). Improving the fundamental understanding of regional seismic signal processing with a unique western United States dataset, in *Proceedings of the 25th Seismic Reearch Review—Nuclear Explosion Monitoring: Building the Knowledge Base*, Vol.2 , pp. 486–484.

Wilcock, W. S. D. and D. R. Toomey (1991). Estimating hypocentral uncertainties for marine microearthquake surveys: A comparison of the generalized inverse and grid search methods, *Mar. Geophys. Res.* 13: pp. 161–171.